IJNAOE
©SNAK, 2015

Int. J. Nav. Archit. Ocean Eng. (2015) 7:873~887
http://dx.doi.org/10.1515/ijnaoe-2015-0061
pISSN: 2092-6782, eISSN: 2092-6790

On the second order effect of the springing response of large blunt ship

Yooil Kim[1] and Sung-Gun Park[2]

[1]*Department of Naval Architecture and Ocean Engineering, Inha University, Incheon, Korea*
[2]*DSME R&D Institute, Daewoo Shipbuilding and Marine Engineering Co., Ltd, Seoul, Korea*

Received 13 June 2014; Revised 6 May 2015; Accepted 5 July 2015

ABSTRACT: *The springing response of a large blunt ship was considered to be influenced by a second order interaction between the incoming irregular wave and the blunt geometry of the forebody of the ship. Little efforts have been made to simulate this complicated fluid-structure interaction phenomenon under irregular waves considering the second order effect; hence, the above mentioned premise still remains unproven. In this paper, efforts were made to quantify the second order effect between the wave and vibrating flexible ship structure by analyzing the experimental data obtained through the model basin test of the scaled-segmented model of a large blunt ship. To achieve this goal, the measured vertical bending moment and the wave elevation time history were analyzed using a higher order spectral analysis technique, where the quadratic interaction between the excitation and response was captured by the cross bispectrum of two randomly oscillating variables. The nonlinear response of the vibrating hull was expressed in terms of a quadratic Volterra series assuming that the wave excitation is Gaussian. The Volterra series was then orthogonalized using Barrett's procedure to remove the interference between the kernels of different orders. Both the linear and quadratic transfer functions of the given system were then derived based on a Fourier transform of the orthogonalized Volterra series. Finally, the response was decomposed into a linear and quadratic part to determine the contribution of the second order effect using the obtained linear and quadratic transfer functions of the system, combined with the given wave spectrum used in the experiment. The contribution of the second order effect on the springing response of the analyzed ship was almost comparable to the linear one in terms of its peak power near the resonance frequency.*

KEY WORDS: Springing; Higher order spectral analysis; Cross bispectrum; Quadratic transfer function; Volterra series.

INTRODUCTION

Hydroelasticity is recognized as one of the main challenges in the design of modern merchant ships, such as ultra large container carriers and very large ore carriers. Hydroelasticity refers to either the resonant vibratory response of the flexible ship structure under a random ocean wave load, or transient vibratory response induced by the impulsive slamming load, which takes place when the ship plunges into the free surface with a wave. The former and latter are called springing and whipping, respectively. Traditionally, the hydroelasticity effect was not considered to be a main design issue until problems were unveiled mostly in the bulk carriers of Greak Lake in 1960s, which ignited some early research efforts on the physics. The importance of hydro-

Corresponding author: *Yooil Kim*, e-mail: *yooilkim@inha.ac.kr*

elasticity has become important since the advent of the larger and faster ships, which has dramatically increased the likelihood of resonance between the ship structure and incoming wave as well as transient vibrations due to the flexibility of the ship.

Considerable research efforts are currently being devoted to the study of hydroelasticity problems to establish a robust design methodology, ultimately targeting the safe operation of unprecedentedly large ships. On the other hand, more research is needed due to the inherent nonlinear nature of the physics behind the hydroelasticity. Some numerical methodologies have been developed under the linear or weakly nonlinear assumption in both the time and frequency domain, the majority of which is based on a combination of potential theory and finite element method (Price and Temarel, 1982; Jensen and Dogliani, 1996; Wu and Moan, 1996; Malenica et al., 2003; Hirdaris et al., 2003; Iijima et al., 2008; Kim et al., 2009; Kim et al., 2013). Efforts have also been made to solve the problem considering the second order interaction between the wave and structure under the potential flow assumption, but the forward speed effect has impeded fruitful research outputs. Computational fluid dynamics coupled with finite element methods is a potentially powerful numerical methodology to solve the problem considering any type of nonlinearities (Oberhagemann et al., 2010; Oberhagemann and Moctar, 2011; Takagi and Ogawa, 2012; Hu et al., 2013). Despite this, the computational demands for obtaining statistically meaningful results under irregular wave using CFD are large, particularly when the focus is on fatigue analysis in which case, all sea states that the ship is exposed to need to be covered.

The model basin test with either a segmented hull model or flexible model is another powerful way to study the hydroelasticity problem. Many model basin tests have been recently carried out (Remy et al., 2006; Iijima et al., 2009; Miyake et al., 2009; Oka et al., 2009; Hong et al., 2011), the majority of which were based on the segmented hull model focusing on measurements of the vibratory behavior of the hull under wave loads. The main focus of the experimental study is normally to obtain the response of a flexible ship under either regular or irregular waves, which are used to validate the numerical analysis results. In some cases, when a more practical output is aimed at, the fatigue damage induced by the hydroelasticity effect was estimated directly under carefully designed test conditions. Storhaug (2007) carried out a systematic experimental test on the segmented scaled model of a large bulk carrier, and claimed that the second order effect related to the diffracted wave near the bow area played an important role in the springing excitation of the flexible ship model. In the experiment, a trial was made to validate the second order effect due to the diffracted wave near the bow by applying different bow segments with different geometries. He also tried to derive the second order transfer function of the system out of the regular wave test, but it was limited to the diagonal component of the transfer function because of the large number of test cases that need to be covered. Unlike the case of a large container carrier, which has a relatively sharp bow shape, this second order effect on springing excitation is more pronounced, particularly when the ship has a blunt bow shape, like ore and bulk carriers. Although the second order effect is influential for the springing excitation of large blunt ship, no study has reported its contribution quantitatively. This study evaluated the relative contribution of both the linear and second order effects in a quantitative manner through a system identification approach. An effort was made to quantify the second order effect through the system identification method, which is based on higher order spectral analysis of the measured test data of the segmented hull model towed a the model basin.

The nonlinear system identification method is generally based on the Volterra series approach. The Volterra series is conceptually similar to the Taylor series in that the system is expressed by the terms of a different order, but distinguishes itself from the Taylor series by the memory effect, which is represented by the convolution integral of the excitation and generalized impulse response functions of each order. The transfer function of each order can be obtained simply by transforming the Volterra kernel to the frequency domain using standard Fourier transform.

The nonlinear system identification on ships and offshore structures under irregular waves has been studied (Hasselmann, 1966; Dalzell, 1975; Pinkster, 1980; Jensen and Pedersen, 1981). Hasselmann (1966) examined the motion response of a ship exposed to the random waves by identifying the Quadratic Transfer Function (QTF), which was obtained by the input-output model. Dalzell (1972) analyzed the added resistance of a ship voyaging through the long-crested random seas by modifying the cross-bispectral analysis proposed by Tick (1961). Dalzell and Kim (1979) examined the second order added resistance problem of a voyaging ship by cross bispectral analysis, under the assumption of a Gaussian input. They reported that the estimated results based on the second order model were in reasonably good agreement with the experimental results. Dalzell (1982; 1984) also proposed the third order model of nonlinear ship responses in irregular seaways. The higher order frequency response function of the considered system was assumed to have a certain form and the probability density function, statistical moments and distribution of extrema were derived.

Choi et al. (1985) applied cross bispectral analysis techniques to the nonlinear response of a moored vessel system in random waves. The second order Volterra series was orthogonalized using Barret's method so that the inter-kernel interference between the linear and second order terms were eliminated, leading to a calculation of the kernels of each order through the inner product. On the other hand, the proposed technique was valid only when the input was Gaussian. Im and Powers (1996) developed an orthogonalized third-order frequency domain Volterra model that was valid both for Gaussian and non-Gaussian excitation. The nonlinear transfer function up to the third order was estimated through a least square fitting of the given input-output data. They also proposed the orthogonal higher order coherence functions through which the contribution of each order can be assessed easily. Adegeest (1997) predicted the nonlinear ship structural response using the third order Volterra model. The starting point of the proposed method lies on the assumption that the higher order frequency response functions can be estimated using zero-memory quadratic and cubic operations, which dramatically simplify the identification process under regular waves of different frequencies. Kim and Kim (2002) analyzed the second order surge force acting on the fixed barge exposed to irregular waves. Cross and cross bispectral analysis was performed to derive both the linear and quadratic transfer functions of the system. Kim and Kim (2004) also analyzed a fixed barge using Gaussian and non-Gaussian approaches and discussed the effects of the significant wave height and data length to be used in the identification process.

The present study combines the cross bispectral analysis technique with the test data of a scaled segmented hull model to identify the second order interaction between the wave and vibrating structure. The measured vertical bending moment at the midship of the segmented hull model was processed and both linear and quadratic transfer functions were derived using cross spectral and cross bispectral analysis to identify the system. The response spectrum of the vibrating ship was then decomposed into a linear and quadratic part to unveil the questionable second order effect potentially induced by the diffraction wave induced by a blunt bow.

THEORETICAL BACKGROUND

Quadratic volterra series and its orthogonalization

Any unknown weakly nonlinear system can be identified using the Volterra series. The Volterra series is a functional series representation of an arbitrary nonlinear system, where a Volterra kernel operates on the system input, producing the system output in terms of its order. The term 'weakly' is inevitably placed in front because the series becomes impractical once the order goes up to take into account the strongly nonlinear effect, eventually becoming of little value. The response, or output of a certain nonlinear system, $y(t)$, under external excitation, $x(t)$, can be expressed in terms of the Volterra series as Eq. (1).

$$y(t) = \sum_{n=0}^{N} \int_{-\infty}^{\infty} \cdots \int_{-\infty}^{\infty} h_n(\tau_1, \tau_2, ..., \tau_n) \prod_{j=0}^{n} x(t-\tau_j) d\tau_j \tag{1}$$

where h_n is nth order Volterra kernel. When N becomes 2, Eq. (1) leads to the second order Volterra series, as shown in Eq. (2).

$$y(t) = h_0 + \int_{-\infty}^{\infty} h_1(\tau_1) x(t-\tau_1) d\tau_1 + \int\int_{-\infty}^{\infty} h_2(\tau_1, \tau_2) x(t-\tau_1) x(t-\tau_2) d\tau_1 d\tau_2 \tag{2}$$

The first term of Eq. (2) is the static bias term. This is related to the statically acting excitation to the system, which can sometimes be excluded assuming that it is known a priori. The second and third terms of Eq. (2) represent the first and second order responses of a given system, which is realized by the convolution integral of the Volterra kernel of each order with the system input. The first order Volterra kernel is an impulse response function of the system and it defines the unique linear characteristics of the system of interest. The second order Volterra kernel is a multi-dimensional generalization of the impulse response function. Once mapped to the particular application handled in this paper, the system response $y(t)$ of Eq. (2) is the vertical midship bending moment and the system input $x(t)$ is the stationary zero mean Gaussian wave excitation.

The series shown in Eq. (2) can be orthogonalized using Barrett's procedure (Choi et al., 1985), which is similar to Wiener's orthogonalization procedure but without the assumption of a white spectrum. For orthogonalization, the mean system response induced by the nonlinearity is extracted from the quadratic term of the Volterra series using relations, such as $E[x(t)] = 0$ and $E[x(t-\tau_1)x(t-\tau_2)] = E[x(\tau_1)x(\tau_2)]$. If an expectation operation is applied to the both sides of Eq. (2), one can obtain the mean system response out of the quadratic term of the Volterra series, and Eq. (2) can be rewritten as,

$$y(t) = \left[h_0 + \int\int_{-\infty}^{\infty} h_2(\tau_1,\tau_2) E[x(\tau_1)x(\tau_2)] d\tau_1 d\tau_2 \right] + \left[\int_{-\infty}^{\infty} h_1(\tau_1)x(t-\tau_1)d\tau_1 \right]$$
$$+ \left[\int\int_{-\infty}^{\infty} h_2(\tau_1,\tau_2)\{x(t-\tau_1)x(t-\tau_2) - E[x(\tau_1)x(\tau_2)]\} d\tau_1 d\tau_2 \right] \tag{3}$$

where $E[\cdot]$ denotes the expectation operation on the quantity inside it. The first bracket of Eq. (3) is composed of a static bias term together with the mean system output, which is extracted out of the quadratic term. Eq. (3) is the orthogonalized quadratic Volterra series because all three terms inside the brackets are orthogonal to each other. The orthogonality can be checked by considering the expected value of the product of any two of the three terms inside brackets, which will always be zero.

If the mean value of the system input is removed, the mean-value-deleted response, $y_0(t) = y(t) - E[y(t)]$ becomes a new system output. In this case, Eq. (3) can be rewritten as

$$y_0(t) = \int_{-\infty}^{\infty} h_1(\tau_1)x(t-\tau_1)d\tau_1 + \int\int_{-\infty}^{\infty} h_2(\tau_1,\tau_2)\{x(t-\tau_1)x(t-\tau_2) - E[x(\tau_1)x(\tau_2)]\} d\tau_1 d\tau_2 \tag{4}$$

Taking a Fourier transform of Eq. (4) gives following frequency domain representation of the quadratic Volterra series, as shown in Eq. (5).

$$Y_0(\omega_m) = H_1(\omega_m)X(\omega_m) + \sum_k \sum_l H_2(\omega_k,\omega_l)\{X(\omega_k)X(\omega_l) - E[X(\omega_k)X(\omega_l)]\} \tag{5}$$

where the summation of second term is done only for $\omega_k + \omega_l = \omega_m$ $X(\omega_m)$ and $Y_0(\omega_m)$ are Fourier transforms of the system input and output, respectively. $H_1(\omega_m)$ and $H_2(\omega_k,\omega_l)$ are the linear and quadratic transfer functions, respectively, which can be obtained by taking a Fourier transform of the Volterra kernel of each order, as shown in Eq. (4).

$$H_1(\omega_1) = \int_{-\infty}^{\infty} h_1(\tau_1) e^{-i\omega_1\tau_1} d\tau_1$$
$$H_2(\omega_1,\omega_2) = \int\int_{-\infty}^{\infty} h_2(\tau_1,\tau_2) e^{-i\omega_1\tau_1 - i\omega_2\tau_2} d\tau_1 d\tau_2 \tag{6}$$

Cross spectral and cross bispectral analysis

Cross spectral and cross bispectral analysis start from Eq. (4), but it requires additional consideration on $x(t)$, which is the zero-mean stationary fluctuation in a Gaussian distribution. The Linear Transfer Function (LTF) in Eq. (5) can be determined once $X^*(\omega_m)$ is multiplied to both sides of Eq. (5). If an expectation operation is applied after multiplication,

$$E\left[Y_0(\omega_m)X^*(\omega_m) \right] = H_1(\omega_m) E\left[|X(\omega_m)|^2 \right]$$
$$+ \sum_k \sum_l H_2(\omega_k,\omega_l) \left\{ E\left[X(\omega_k)X(\omega_l)X^*(\omega_m) \right] - E\left[X(\omega_k)X(\omega_l) \right] E\left[X^*(\omega_m) \right] \right\} \tag{7}$$

The last two terms of Eq. (7) vanish, i.e. $E\left[X(\omega_k)X(\omega_l)X^*(\omega_m)\right]=0$ and $E\left[X(\omega_k)X(\omega_l)\right]=0$, because $x(t)$ is zero-mean stationary Gaussian fluctuation (Choi et al., 1985). This simplification is possible because all the spectral components of different frequencies become independent of each other if $x(t)$ is a zero-mean stationary Gaussian fluctuation. Therefore, Eq. (7) finally leads to the well-known formula, as shown in Eq. (8).

$$H_1(\omega_m)=\frac{E\left[Y_0(\omega_m)X^*(\omega_m)\right]}{E\left[\left|X(\omega_m)\right|^2\right]} \tag{8}$$

The numerator of Eq. (8) is the cross spectrum of the input and output of a given system and LTF is defined as the normalized value of a cross spectrum with respect to the auto spectrum of the input.

Quadratic Transfer Function (QTF) can be deduced by Eq. (8) in a similar manner, but this time after multiplying both sides of the equation by $X^*(\omega_i)X^*(\omega_j)$, where $\omega_i+\omega_j=\omega_m$. Again, if an expectation operation is applied after multiplication,

$$E\left[Y_0(\omega_m)X^*(\omega_i)X^*(\omega_j)\right]=H_1(\omega_m)E\left[X(\omega_m)X^*(\omega_i)X^*(\omega_j)\right]$$

$$+\sum_k\sum_l H_2(\omega_k,\omega_l)\left\{E\left[X(\omega_k)X(\omega_l)X^*(\omega_i)X^*(\omega_j)\right]-E\left[X(\omega_k)X(\omega_l)\right]E\left[X^*(\omega_i)X^*(\omega_j)\right]\right\} \tag{9}$$

Considering the stationarity and Gaussianity of $x(t)$, whose mean is zero, one has $E\left[X(\omega_m)X^*(\omega_i)X^*(\omega_j)\right]=0$, which means that the first term of RHS vanishes. For the last term of Eq. (9) inside $\{\cdot\}$, following relationships are employed:

$$E\left[X(\omega_k)X(\omega_l)X^*(\omega_i)X^*(\omega_j)\right]-E\left[X(\omega_k)X(\omega_l)\right]E\left[X^*(\omega_i)X^*(\omega_j)\right]$$

$$=\begin{cases}0 & if\ (\omega_k,\omega_l)\neq(\omega_i,\omega_j)\\ \left|X(\omega_i)X(\omega_j)\right|^2 & if\ (\omega_k,\omega_l)=(\omega_i,\omega_j)\end{cases} \tag{10}$$

Finally, Eq. (9) is simplified as

$$E\left[Y_0(\omega_m)X^*(\omega_i)X^*(\omega_j)\right]=H_2(\omega_i,\omega_j)\left|X(\omega_i)X(\omega_j)\right|^2 \qquad \omega_i+\omega_j=\omega_m,\quad \omega_i\geq\omega_j \tag{11}$$

Hence, QTF of a given system is given by the following:

$$H_2(\omega_i,\omega_j)=\frac{E\left[Y_0(\omega_m)X^*(\omega_i)X^*(\omega_j)\right]}{\left|X(\omega_i)X(\omega_j)\right|^2} \qquad \omega_i+\omega_j=\omega_m,\quad \omega_i\geq\omega_j \tag{12}$$

where the numerator is the cross bispectrum of the input and output of a given system and QTF is defined as the normalized value of cross bispectrum with respect to the cross spectrum of the input. The cross bispectrum shown in Eq. (12) is a measure of the quadratic nonlinear interaction between the input and output, and is defined as a Fourier transform of a third cumulant, as shown in Eq. (13).

$$C_3(\tau_1,\tau_2)=E\left[y(t)x(t+\tau_1)x(t+\tau_2)\right] \tag{13}$$

MODEL TEST

To analyze the second order effects of the hydroelastic response of a large blunt ship, the experimental data obtained from the model basin test was used to identify the transfer functions up to the second order. The scale segmented model of a Very Large Ore Carrier (VLOC) with a 400,000 *ton* dead weight was towed in a model basin under the given wave conditions. Table 1 summarizes the main particulars of the tested ship.

Fig. 1 shows the backbone system installed on the hull together with the hull segmentation. The hull and backbone system were segmented into 6 pieces and load cells were installed at each connection of the backbone system to measure both the vertical shear force and bending moment. Cuts 1 and 5 are rigid connections, and only the vertical shear forces are measured at this location. Cuts 2 to 4 are the flexible connections and both vertical bending moment and shear forces are measured. The backbone system is a tripod type truss structure and a special connection structure was inserted at each connection so that the stiffness of the connection could be adjustable, allowing tuning of the natural frequency of the model. The mass distribution of the full scale ship was reflected in the model ship by placing mass blocks at designated locations inside the model ship to match the longitudinal mass distribution of a full scale ship.

Table 1 Main particulars of VLOC.

Items	Value
Length between perpendiculars [*m*]	350.00
Breadth molded [*m*]	65.00
Depth molded [*m*]	30.40
Displacement [*tones*] – Port loaded	448,751
Mean draft [*m*] – Port loaded	23

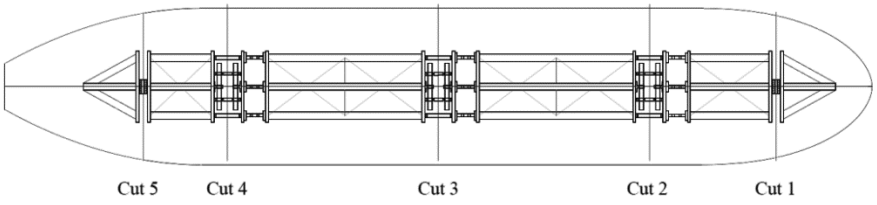

(a) Top view.

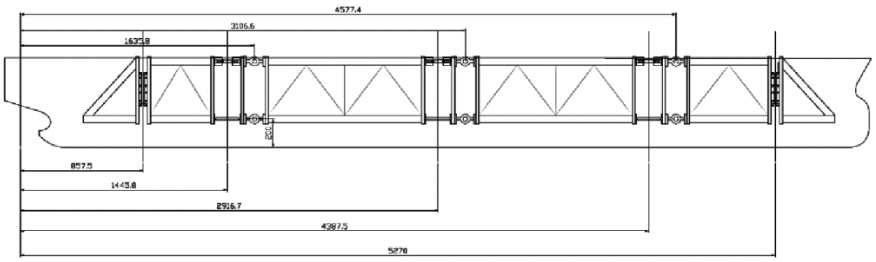

(b) Side view.

(c) Model.

Fig. 1 Test model (1/60 scale).

The scale ratio of the model was set to 60, which was determined based on the quality-guaranteed minimum wavelength of the model basin. Both the time and length of the model were determined according to the Froude scale law. Hence, the model towing speed and natural frequency of the model ship were set as follows:

$$V_m = V_f \sqrt{\frac{L_m}{L_f}} = \frac{V_f}{\sqrt{\Lambda}} \qquad \omega_m = \omega_f \sqrt{\frac{L_f}{L_m}} = \omega_f \sqrt{\Lambda} \tag{14}$$

where subscript m means the model ship, whereas f means the full scale ship. Λ is the scale ratio, ω is the circular frequency and L is the length of the ship. The stiffness of the model ship was also scaled down according to the relationship given in Eq. (14) together with the frequency of a homogeneous beam. Therefore, the bending stiffness of the model ship was set to

$$EI_m = EI_f \frac{\rho_m}{\rho_f \Lambda^5} \tag{15}$$

where EI is the bending stiffness of the ship and ρ is the density of the material. Only the vertical flexibility was considered in the model ship because the ship was planned to be towed under head wave conditions.

The model ship was calibrated in such a way that it reproduced the dynamic characteristics of the full scale ship, particularly the natural frequencies. The expected wet natural frequencies of the model ship under full load conditions corresponds to 0.37 *Hz* and 0.78 *Hz* for the first and second vertical vibration modes, respectively. These values are the natural frequencies of the model ship, which were obtained by scaling down the values calculated by the numerical wet hammering test done by WISH-Flex program (Kim, 2009). By targeting the expected wet natural frequency of the model ship for the first vertical vibration mode, the stiffness of the model ship was adjusted using the special connection structure, and the wet natural frequencies of 0.37 *Hz* and 0.88 *Hz* for the first and second vertical vibration mode were achieved. The distribution of mass along the ship length was determined by following that of a real ship. Owing to the dominant effect of the first vertical vibration mode to the response of the model ship, the first mode was exclusively respected during the calibration process. No intentional damping calibration was made for the model ship, because the damping ratio of the full scale ship is unknown. The damping ratio of the model ship was 0.4~0.6% under wet conditions, to which both the structural and hydrodynamic damping contributed. The calibrated model ship was towed in a model basin through an irregular head wave at a given speed. The irregular waves were generated based on the JONSWAP wave spectrum given in Eq. (16).

$$S(\omega) = \frac{\alpha g^2}{\omega^5} \exp\left[-\frac{4}{5}\left(\frac{\omega_p}{\omega}\right)^4\right] \gamma^{\exp\left[-\frac{(\omega-\omega_p)^2}{2\omega_p^2\sigma^2}\right]}$$

$$\alpha = \frac{5}{16}\frac{H_s^2 \omega_p^2}{g^2}\left(1 - 0.287\ln(\gamma)\right), \quad \sigma = \begin{cases} 0.07 \ if \ \omega \le \omega_p \\ 0.09 \ if \ \omega \le \omega_p \end{cases} \tag{16}$$

Three sea states were selected for the analysis, which are the cases that the relative contribution of the springing response is significant compared to the quasi-static wave induced response. Table 2 lists the 3 selected sea states, all of which have a relatively short wave period. Significant springing excitation can be expected from these sea states owing to the less dramatic wave energy decreasing pattern near the tail of the wave spectrum. The towing speed was decreased gradually with increasing significant wave height considering both the added resistance and voluntary speed reduction. The port loaded condition was considered, so that the potential bottom-slamming-induced whipping response does not prevail, in which case, the validity of the spectral analysis is questioned.

Table 2 Analyzed test conditions.

Sea state No.	γ	$H_s\,[m]$	$T_p\,[sec]$	Speed [*kts*]
1	3	4.5	8.6	12.0
2	5	6.5	8.2	8.0
3	5	8.5	8.2	6.0

Fig. 2 shows the measured time history of the wave elevation and vertical bending moment at midship section of the hull under sea states No.1 and No.2. For clear visibility, data is plotted between 500 to 1,000 *sec* in a selective manner, out of test data of 35 *min*. in a full scale time frame. Fig. 2(a) to (c) clearly indicate that the vibration response is significant. The entire measured data out of the model test were scaled up, so that the values are full scale ones.

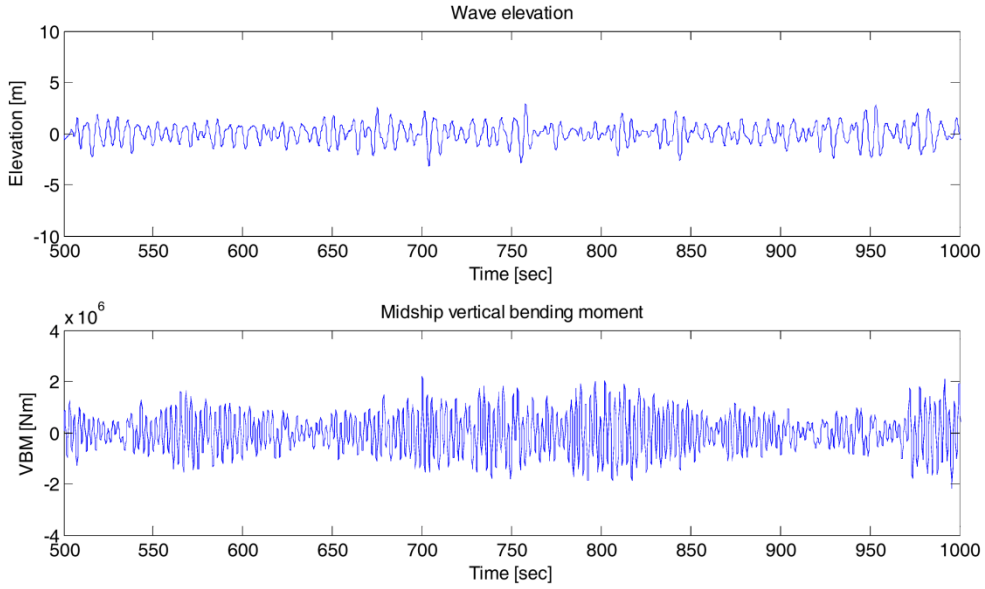

(a) Sea state No.1 (H_s=4.5 *m*, T_p=8.6 *sec*).

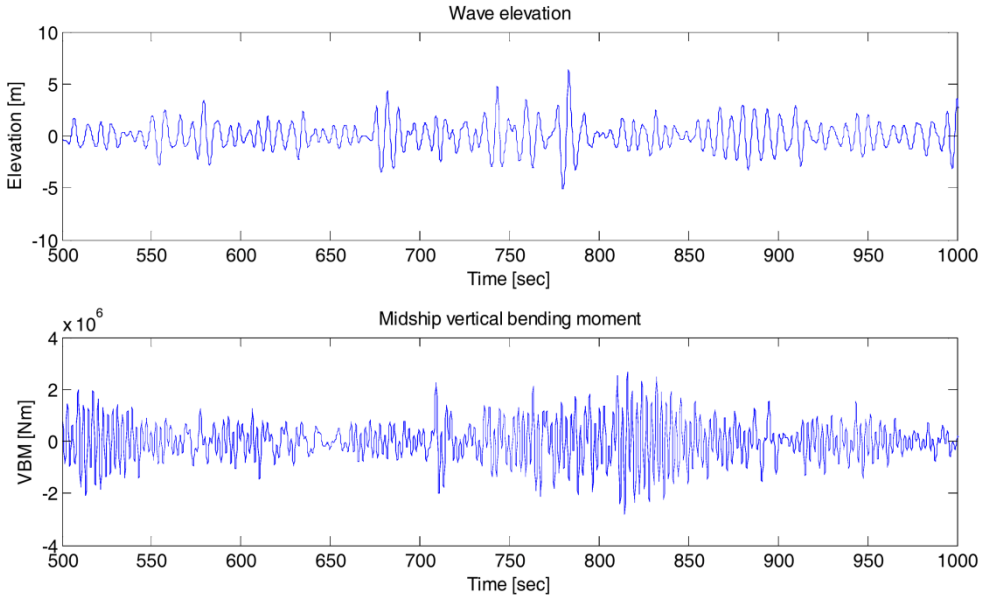

(b) Sea state No.2 (H_s=6.5 *m*, T_p=8.2 *sec*).

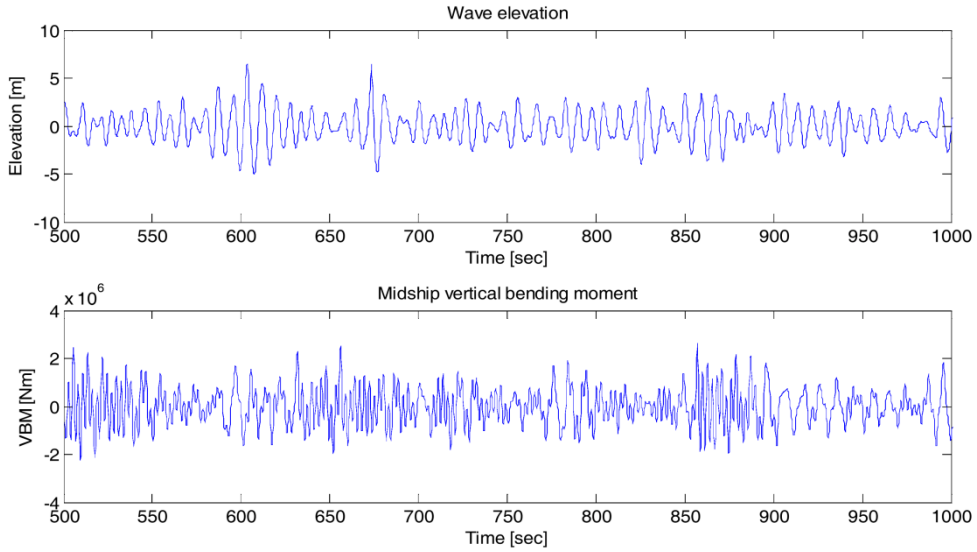

(c) Sea state No.3 (H_s=8.5 *m*, T_p=8.2 *sec*).

Fig. 2 Measured time history of the wave elevation and vertical bending moment.

Fig. 3 shows both the wave and VBM spectral mass functions for each sea state, which is expressed as the frequency of the encounter. Regarding the wave spectrum, the peak modal frequency tends to shift to the low frequency direction as the wave height increases, which is caused by the decreasing ship speed with respect to the increasing wave height. In terms of the VBM response, the response spectrum in the wave frequency regime tends to increase with increasing wave height, as expected, but this tendency does not hold for the high frequency vibration response. If the peak value of the high frequency response is focused, the high frequency vibration response tends to stay relatively calm regardless of the wave height variation. This appears to be caused by the compensation between the positive and negative effects, each of which is induced by an increase in wave height and a decrease in speed. Speed reduction with respect to the wave height causes the wave spectrum to shift toward the low frequency direction, eventually leading to less excitation of the wave to the vibration response, at least in a linear sense.

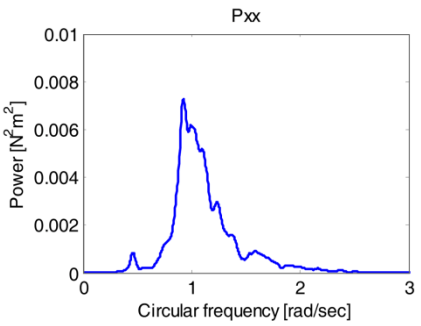

(a) Wave spectrum (Sea state No.1).

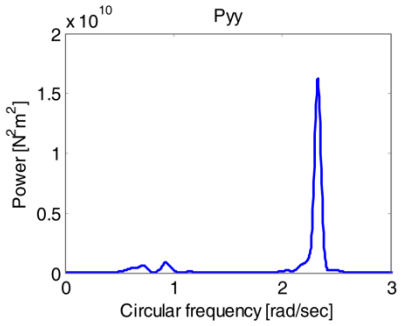

(b) VBM spectrum (Sea state No.1).

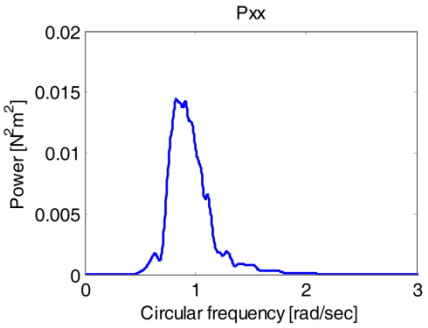

(c) Wave spectrum (Sea state No.2).

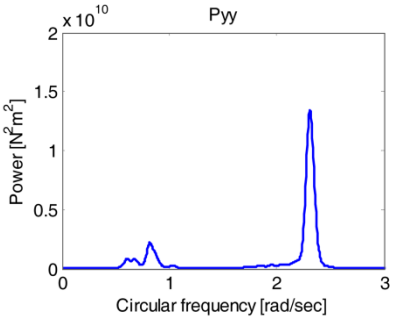

(d) VBM spectrum (Sea state No.2).

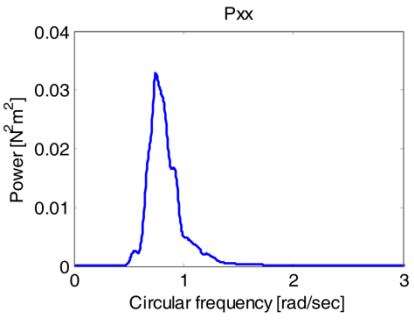

(e) Wave spectrum (Sea state No.3).

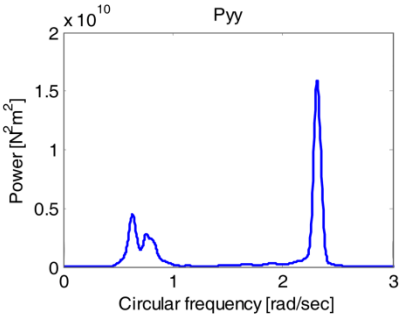

(f) VBM spectrum (Sea state No.3).

Fig. 3 Wave and VBM response spectrum for each sea state.

Throughout all cases considered, the vibration responses were more pronounced compared to the response in the wave frequency regime, even though the wave energy appears to be barely present in this frequency regime. The significance of wave energy near the tail of wave spectrum in terms of vibration response is normally difficult to recognize, but the following cross spectral analysis can identify it clearly.

HIGHER ORDER SPECTRAL ANALYSIS

Cross spectral analysis for the LTF

Using the measured time history of both the wave elevation and VBM at the midship section, cross spectral analysis was carried out to identify the LTF. As explained before, the LTF can be obtained by normalizing the cross spectrum of the wave elevation and VBM response with an auto spectrum of the wave elevation. Fig. 4 shows the cross spectra and LTFs for each sea state. The cross spectrum shown in Fig. 4 is a measure of the correlation between the wave elevation and the VBM response, indicating that high power means a strong correlation between the two quantities at a given frequency in a linear manner. Fig. 4(a), (c) and (e) show that there is a strong correlation between the wave elevation and VBM response within the wave frequency regime, which in turns means that wave induced VBM response is linearly correlated with the wave elevation. Another peak of power appears around the frequency value of 2.3 *rad/sec*, which is induced by the vibration response correlated with the wave elevation. Normalizing the cross spectrum of wave elevation and VBM response to the auto power spectrum of the wave elevation leads to the VBM response intensity with respect to the unit wave elevation. These linear transfer functions are plotted in Fig. 4(b), (d) and (f). A high peak appears around the frequency of 2.3 *rad/sec*, which is driven by the vibration response of the hull excited by the wave of the same frequency. Owing to the different ship speeds for different sea state, the LTFs from the different sea states did not match each other. Interestingly, the discrepancy of LTFs within vibration frequency is not as signify-cant as that of wave frequency. In terms of the peak frequency in the vibration frequency regime, it is natural to expect that the peak frequency matches the natural frequency of the flexible hull, which is the case for all three LTFs. In case of the VBM response in the wave frequency regime, both the peaks and magnitudes change depending on the ship speed because, for example, the heave or pitch resonance frequency moves when the ship speed changes, eventually influencing the VBM response.

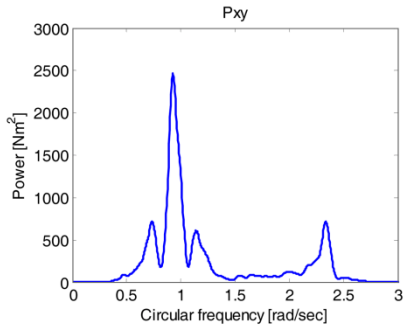

(a) Cross spectrum (Sea state No.1).

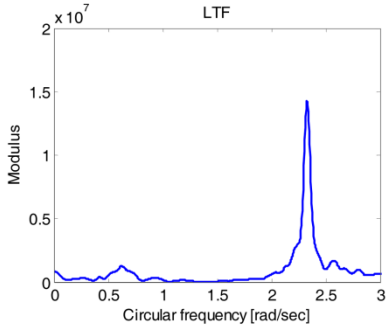

(b) LTF (Sea state No.1).

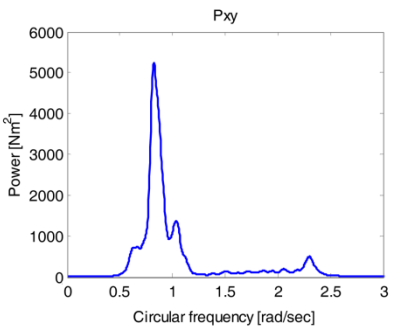

(c) Cross spectrum (Sea state No.2).

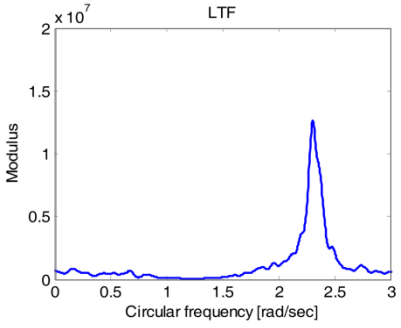

(d) LTF (Sea state No.2).

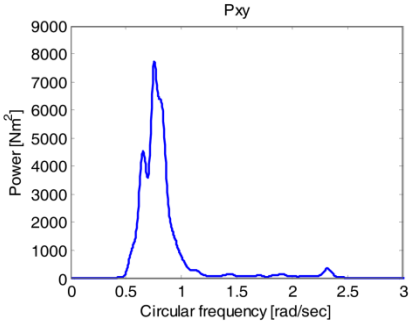

(e) Cross spectrum (Sea state No.3).

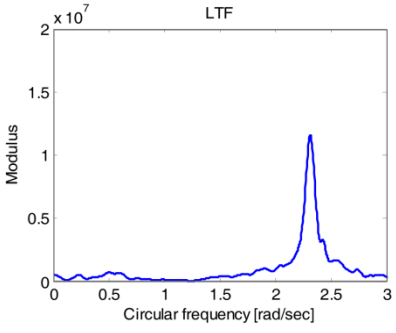

(f) LTF (Sea state No.3).

Fig. 4 Cross spectrum and linear transfer function.

Cross bispectral analysis for QTF

To decompose the response spectrum into its linear and quadratic portions, QTF was identified using cross bispectral analysis applied to the measured wave elevation and VBM response time history. QTF is defined as the normalized cross bispectrum with respect to the cross spectrum of the wave elevation. The cross bispectrum in Fig. 5 is a measure of the quadratic correlation between the VBM response and wave elevation, indicating that high power means a strong correlation between the VBM response at a given frequency (ω_m) and the wave elevation of two frequencies (ω_i, ω_j), whose sum or difference matches the frequency of VBM. In Fig. 5(a), (c) and (e), some typical pattern of cross bispectrum can be observed. A relative high power concentration appears along the straight line, $\omega_1 + \omega_2 = 2.3$ *rad/sec*, which means that the wave elevation and vibration response have a strong quadratic sum frequency interaction. More specifically, this power concentration along the line, $\omega_1 + \omega_2 = 2.3$ *rad/sec*, within the frequency range, 0.5 to 1.5 *rad/sec*, is induced by the higher power of the wave spectrum in the corresponding frequency range. In addition, the power concentration in the first and third quadrants suggests that the quadratic interaction between the wave elevation and the VBM response is takes place only in the sum frequency sense. Furthermore, a relatively small power concentration is present along the straight line of $\omega_1 + \omega_2 = 0.5 \sim 1.0$ *rad/sec*, which is the quadratic difference frequency interaction between the wave elevation and wave frequency response.

Once normalized, these cross bispectra become QTFs, as shown in Fig. 5(b), (d) and (f). The contour plots of QTF indicate that a high magnification is expected along the line, $\omega_1 + \omega_2 = 2.3$ *rad/sec*, within the frequency range of 0.5 to 1.5 *rad/sec*. Similar to the high peaks of LTFs around the frequency of 2.3 *rad/sec*, these 2D peaks, when combined with the cross spectrum of wave elevation, are considered a source of a significant second order response in the vibration frequency regime. The contribution of the second order respons e is expected to be considerable because the peaks run with the same magnitude along the line of $\omega_1 + \omega_2 = 2.3$ *rad/sec*, particularly within the frequency range of 0.5 to 1.5 *rad/sec*, where the power of wave elevation is highly concentrated.

Additional isolated peaks lying on the $\omega_1 + \omega_2 = 0.5 \sim 1.0$ *rad/sec* on the second and fourth quadrants are the source of the second order response in the wave frequency regime, but the contribution of this second order effect is considered to be limited because the these peaks are spotted on the plane unlike those in the vibration frequency regime.

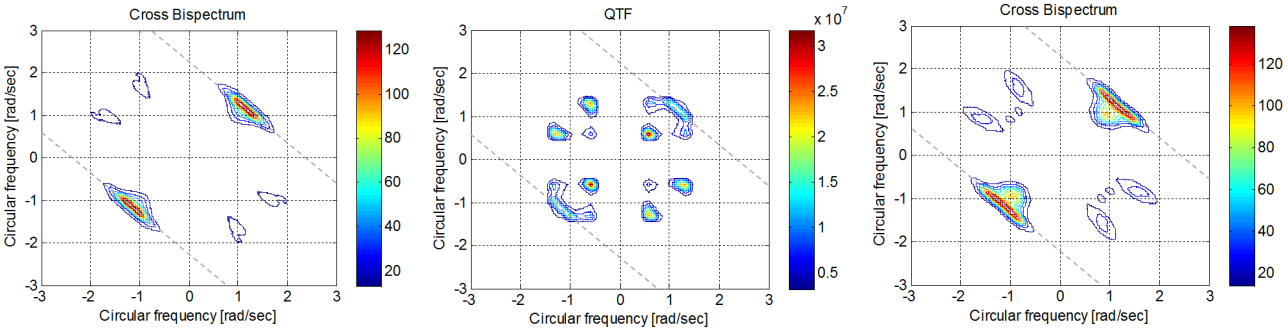

(a) Cross bispectrum (Sea state No.1). (b) QTF (Sea state No.1). (c) Cross bispectrum (Sea state No.2).

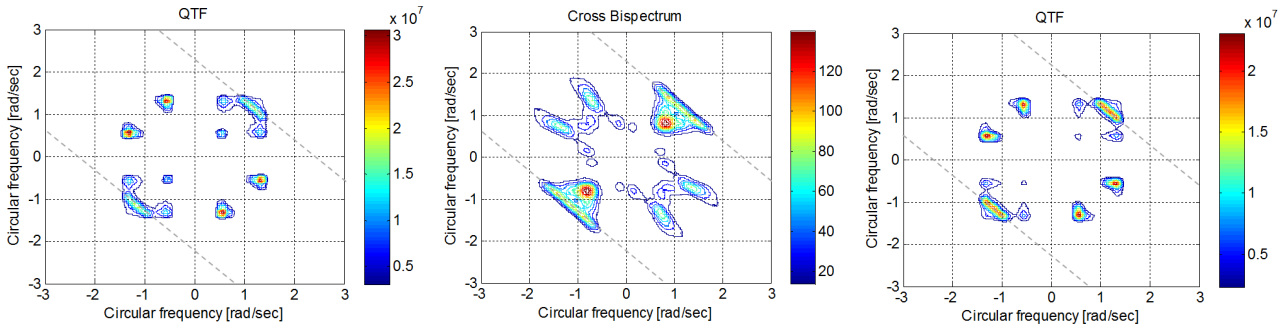

(d) QTF (Sea state No.2). (e) Cross bispectrum (Sea state No.3). (f) QTF (Sea state No.3).

Fig. 5 Cross bispectrum and quadratic transfer function.

Response decomposition

Eq. (17) shows the relationship between the wave spectrum and the response spectrum considering both the linear and quadratic interaction between the input and output. The first term is the well-known expression of the response spectrum, which is valid only if the system under consideration is linear. The second term represents the second order response spectrum that is expressed in terms of the integration of the product of QTF and cross spectrum of the wave elevation. The integration of Eq. (17) is done along the straight line of $\omega_1 + \omega_2 = const$.

$$S_{yy}(\omega) = |H_1(\omega)|^2 S_{xx}(\omega) + \frac{1}{\pi}\int_{-\infty}^{\infty} |H_2(\omega-\theta,\theta)|^2 S_{xx}(\omega-\theta) S_{xx}(\theta) d\theta \tag{17}$$

Fig. 6 presents the VBM response spectra for each sea state decomposed into linear and linear plus quadratic responses. For better visibility, the frequency range was divided into the wave and vibration frequency, respectively, with a dividing frequency of 1.5 *rad/sec*. For all cases, the linear responses, which are represented by the red line, fall short of the measured responses, the blue line. On the other hand, the discrepancies between the measurements and analysis results become small once the quadratic parts are added to the linear ones. When focus is on the peak value of the response spectrum in the vibration frequency regime, it can be observed that the relative contribution of the quadratic part is significant and it tends to increase slightly as the wave height increases. On the other hand, there still remain some gaps between the measurement and analysis results, even after adding the quadratic part, and this gap tends to become larger as the wave height increases, from No.1 to No.3. This reaming gap is understood as what might be filled even with higher order effects.

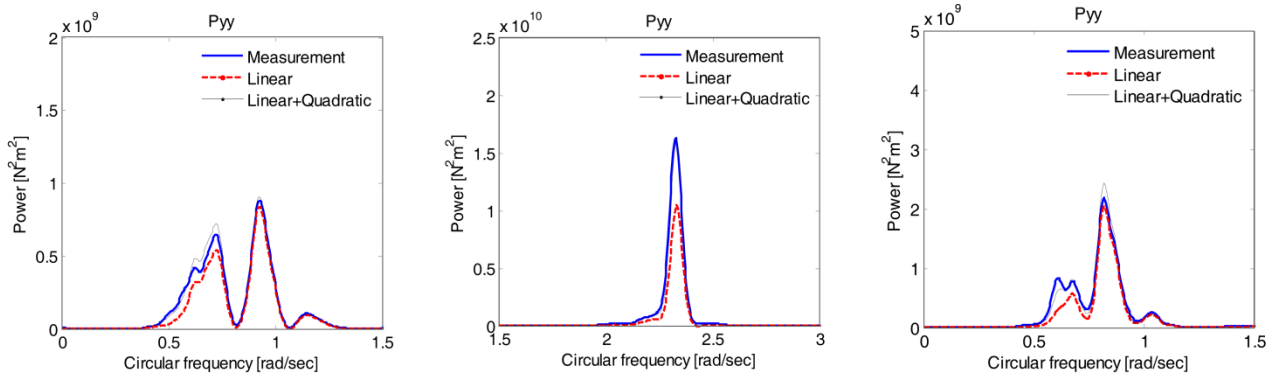

(a) Wave frequency (Sea state No.1). (b) Vibration frequency (Sea state No.1). (c) Wave frequency (Sea state No.2).

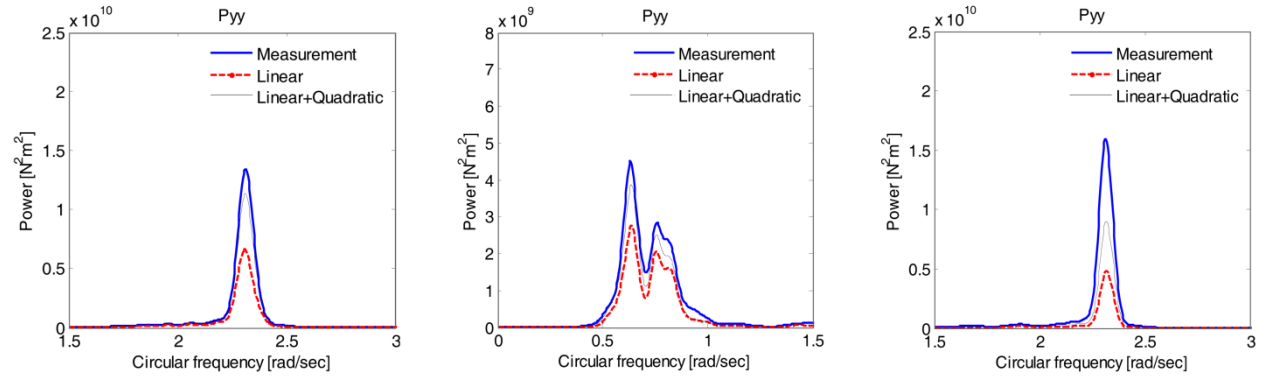

(d) Vibration frequency (Sea state No.2). (e) Wave frequency (Sea state No.3). (f) Vibration frequency (Sea state No.3).

Fig. 6 Decomposition of the VBM response spectrum for each sea state.

Turning to the responses in wave frequency regime, the influence of quadratic nonlinearity is less pronounced, compared to those in the vibration frequency regime. This is understandable because the hull geometry of an analyzed ship is unlikely to

induce a significant nonlinear effect, which may be caused by a dramatic change in wet hull geometry during the motion. The response spectra predicted by spectral analysis do not match the measurements precisely particularly in the wave frequency regime, and this is related to the accuracy of the QTFs. The accuracy of QTF is strongly related to the stationarity and Gaussianity of the wave elevation, but the Gaussianity assumption does not hold in a strict sense once the wave elevation becomes large. Another potential source of error in predicting the QTF in the wave frequency regime is the length of data used for cross bispectral analysis. No systematic study on the effects of the data length for accurate spectral analysis has been carried out, which is considered one of the most important future study items. Although there still is room for further improvement of the prediction accuracy, the analysis results shown in Fig. 6 clearly indicate that the second order effects on the vibration response are considerable, which might be caused by the nonlinear diffraction forces present mainly near the bow of the ship.

CONCLUSIONS

The unknown second order effect related to the springing response of a large blunt ship, such as very large ore carrier, was analyzed using the higher order spectral analysis. Based on the above mentioned numerical results and discussions, the following conclusions were derived

1) The second order effects of the springing response of a very large ore carrier was analyzed using higher order spectral analysis. The VBM response spectrum, which was obtained from the segmented model test, was decomposed into linear and linear plus quadratic parts using the linear and quadratic transfer functions derived from cross and cross bispectral analysis.
2) The VMB response spectra under the considered sea states showed that the vibration response is quite pronounced even though the power of wave elevation at the corresponding frequency regime is negligibly small. This in turns indicates the presence of a significant second order effect relevant to the vibration response of the hull.
3) Cross spectral analysis showed that there is some linear correlation between the VBM response and wave elevation in the vibration frequency regime, even though the wave energy barely exists. A normalized version of the cross spectrum, i.e. LTF, clearly indicated that a high magnification is expected in the vibration frequency regime.
4) The cross bispectral analysis results showed that the strong quadratic interaction between the VBM response and wave elevation is present along the line, $\omega_1 + \omega_2 = 2.3$ *rad/sec*, which corresponds to the natural frequency of the ship. QTF also indicated that a high magnification is expected along this line, which can lead to significant second order effects in terms of the vibration response.
5) The quadratic part of vibration response was comparable to the linear one and the relative contribution of the quadratic part tended to increase with increasing wave height. On the other hand, the contribution of the quadratic part in the wave frequency regime is limited, which is considered natural owing to the relatively mild geometric changes to the wet surface with respect to the ship motion.
6) In this paper, the cross and cross bispectral analysis technique was applied successfully to identify the second order effect of the springing response of a large blunt ship. This methodology can be extended to cover full scale measurement data, so that an unknown nonlinear effect related to the springing response of large merchant ships can be understood with clarity, eventually supporting the robust ship design against potential damage induced by the springing response.

ACKNOWLEDGEMENT

This study was supported by a Special Education Program for Offshore Plant by the Ministry of Trade, Industry and Energy Affairs (MOTIE). Author also wish to thank Daewoo Shipbuilding and Marine Engineering Co. Ltd. for providing the experimental data and supporting the work.

REFERENCES

Adegeest, A., 1997. Third-order Volterra modeling of ship responses based on regular wave results. *Twenty-First Symposium on Naval Hydrodynamics*, Trondheim, Norway, June 1997.

Choi, D.W., Miksad, R.W. and Powers, E.J., 1985. Application of digital cross-bispectral analysis techniques to model the

non-linear response of a moored vessel system in random seas. *Journal of Sound and Vibration*, 99(3), pp.309-326.

Dalzell, J.F., 1972. *Application of cross-bi-spectral analysis to ship resistance in waves*, *SIT-DL-72-1606.* NJ: Stevens Institute of Technology.

Dalzell, J.F., 1975. *The applicability of the functional polynomial input-output model to ship resistance in waves, Technical Report SIT-DL-75-1974*. Hoboken, New Jersey: Stevens Inst. of Technology.

Dalzell, J.F., 1982. *An investigation of the applicability of the third degree functional polynomial model of nonlinear ship motion problems, Technical Report SIT-DL-82-9-2275*. Hoboken, New Jersey: Stevens Inst. of Technology.

Dalzell, J.F., 1984. *Approximations to the probability density of maxima and minima of the response of a nonlinear system, Technical Report EW-22-84*. Annapolis, Maryland: US Naval Academy.

Dalzell, J.F. and Kim, C.H., 1979. An analysis of quadratic frequency response for added resistance. *Journal of Ship Research*, 23(23), pp.198-208.

Hasselmann, K., 1966. On nonlinear ship motions in irregular waves. *Journal of Ship Research*, 10, pp.64-68.

Hirdaris, S.E., Price, W.G. and Temarel, P., 2003. Two- and three-dimensional hydroelastic analysis of a bulker in waves. *Marine Structures*, 16, pp.627-658.

Hong, S.Y., Kim, B.W. and Nam, B.W., 2011. Experimental study on torsion springing and whipping of a large container ship. *Proceedings of the Twenty-first (2011) International Offshore and Polar Engineering Conference*, Maui, Hawaii, USA, 19-24 June 2011, pp.486-494.

Hu, C., Liao, K. and Duan, W., 2013. CFD simulation of flexible ship in regular head waves. *Proceeedings of the 32nd International Conference on Ocean*, *Offshore and Arctic Engineering,* Nantes, France, June 2013.

Iijima, K., Yao, T. and Moan, T., 2008. Structural response of a ship in severe seas considering global hydroelastic vibrations. *Marine Structures*, 21, pp.420-445.

Iijima, K., Hermundstad, O.A., Zhu, S. and Moan, T., 2009. Symmetric and antisymmetric vibrations of a hydroelastically scaled model. *Proceedings of the 5th International Conference on Hydroelasticity in Marine Technology*, Southampton, UK, September 2009.

Im, S. and Powers, E.J., 1996. A sparse third-order orthogonal frequency-domain Volterra-like model. *Journal of The Franklin Institute*, 333, pp.385-412.

Jensen, J.J. and Pedersen, P.T., 1981. Bending moments and shear forces in ships sailing in irregular waves. *Journal of Ship Research*, 25, pp.243-251.

Jensen, J.J. and Dogliani, M., 1996. Wave-induced ship hull vibrations in stochastic seaways. *Marine Structures*, 9, pp.353-387.

Kim, N.S. and Kim, C.H., 2002. Cross-bi-spectral estimation of nonlinear force on fixed structure in nonlinear waves. *Proceedings of 12th International Offshore and Polar Engineering Conference*, Kitakyushu, Japan, June 2002.

Kim, N.S. and Kim, C.H., 2004. Gaussian and nonGaussian input method for extraction of QTFs from test data of offshore structures. *Proceedings of 14th International Offshore and Polar Engineering Conference*, Toulon, France, June 2004.

Kim, Y., 2009. *Time domain analysis on hull-girder hydroelasticity by fully coupled BEM-FEM approach*. PhD Thesis. Seoul National University.

Kim, Y.I, Kim, K.H. and Kim, Y.H., 2009. Springing analysis of a seagoing vessel using fully coupled BEM-FEM in the time domain. *Ocean Engineering*, 36, pp.785-796.

Kim, K.H., Bang, J.S., Kim J.H., Kim, Y., Kim, S.J. and Kim, Y., 2013. Fully coupled BEM-FEM analysis for ship hydro-elasticity in waves. *Marine Structures*, 33, pp.71-99.

Malenica, S., Molin, B. and Senjanociv, I., 2003. Hydroelastic response of a barge to impulsive and non-impulsive wave loads. *Proceedings of the 3rd International Conference on Hydroelasticity in Marine Technology*, Oxford, UK, September 2003.

Miyaka, R., Matsumoto, T., Zhu, T., Usami, A. and Dobashi, H., 2009. Experimental studies on the hydroelastic response using a flexible mega-container ship model. *Proceedings of the 5th International Conference on Hydroelasticity in Marine Technology*, Southampton, UK, September 2009.

Oberhagemann, J., Moctar, O. and Rathe, H., 2010. Fluid-structure interaction using free-surface RANSE for springing and whipping. *Proceedings of the 13th Numerical Towing Tanks Symposium*, Duisburg, Germany, October 2010.

Oberhagemann, J. and Moctar, O., 2011. Numerical and experimental investigation of whipping and springing of ship

structures. *Proceedings of the 21st International Offshore and Polar Engineering Conference*, Maui, USA, June 2011.

Oka, M., Oka, S. and Ogawa, Y., 2009. An experimental study on wave loads of a large container ship and its hydroelastic vibration. *Proceedings of the 5th International Conference on Hydroelasticity in Marine Technology*, Southampton, UK, September 2009.

Pinkster, J.A., 1980. *Low frequency second order wave exciting forces on floating structures*. PhD thesis. Technical University of Delft.

Price,W.G. and Temarel, P., 1982. The influence of hull flexibility in the anti-symmetric dynamic behavior of ships in waves. *International Shipbuilding Progress*, 29.

Remy, F., Molin, B. and Ledoux, A., 2006. Experimental and numerical study of the wave response of a flexible barge. *Proceedings of the 4th International Conference on Hydroelasticity in Marine Technology*, Wuxi, China, September 2006.

Storhaug, G., 2007. *Experimental investigation of wave induced vibrations and their effect on the fatigue loading of ships*. Ph.D. Thesis. Norwegian University of Science and Technology.

Takagi, K. and Ogawa, Y., 2012. Hydroelasticity in marine technology. *Proceedings of the 16th International Conference on Hydroelasticity in Marine Technology*, Tokyo, Japan, September 2012.

Tick, L.J., 1961. The estimation of the transfer functions of quadratic systems. *Technometrics*, 3(4), pp.563-567.

Wu, M.K. and Moan, T., 1996. Linear and nonlinear hydroelastic analysis of high-speed vessel. *Journal of Ship Research*, 40(2), pp.149-163.